On the Capacity Gain from Full Duplex Communications in a Large Scale Wireless Network

Xudong Wang, *Senior Member, IEEE*, Huaiyu Huang, and Taewon Hwang

Abstract—Compared to half duplex communications, full duplex communications can significantly improve link capacity. However, in a large scale wireless network such as a wireless mesh network, the capacity gain from full duplex communications has not been fully investigated. To this end, a metric of network capacity called transmission capacity is studied in this paper for a full duplex wireless network. It captures the maximum transmission throughput in a unit area, subject to a certain outage probability. The key challenge of deriving transmission capacity is to characterize the aggregate interference of the typical link in a full duplex wireless network, which is completely different from that in a half duplex wireless network. In this paper, stochastic geometry is employed to model the network topology as a Thomas cluster point process and then the aggregate interference is characterized as a shot-noise process. Based on these models, the transmission capacity is derived. Analytical results show that under the same network density the distribution of aggregate interference in a full duplex wireless network is more dispersed than that in a half duplex wireless network. Comparisons of transmission capacity between a full duplex network and a half duplex network reveal that the capacity gain from full duplex communications is limited due to severe aggregate interference. This result implies that self-interference cancellation alone cannot ensure scalable full duplex wireless networking.

Index Terms—Full duplex wireless communication, stochastic geometry, Thomas cluster point process, transmission capacity

1 Introduction

To improve spectrum efficiency of a radio, advanced self-interference cancellation technologies [1], [2], [3], [4], [5] have been invented to achieve full duplex wireless communications, i.e., simultaneous transmission and reception in the same frequency. Moreover, techniques for full duplex MIMO [5] and in-band full duplex WiFi radios [6] have also been developed.

With full duplex wireless communications, link capacity can be significantly improved. Practical implementation shows that 84 percent improvement of link throughput can be achieved [2]. However, in a large scale wireless network, how much capacity gain can be achieved is hard to be determined. In [7], a wireless network with three nodes, one full duplex access node and two half duplex nodes, is studied, and the achievable rate of this network is derived. In [8] throughput gain of a MIMO wireless system with full duplex radios is analyzed in a single cell wireless network. Moreover, Contraflow [9] and FD-MAC [10] are designed to improve the network throughput of a full duplex wireless network, but these analytical frameworks are proposed for specific network topologies. In [11], end-to-end delay and throughput are analyzed for a multi-hop network. However, the analytical model is based on the assumption that, an interfering pair of nodes in a full duplex network are located at the same position asymptotically as network density approaches zero. Thus, it cannot reveal the network throughput gain for a large scale full duplex wireless network. As a result, for a large scale wireless network, how to determine the capacity gain from full duplex communications remains a challenging problem. In [12], an upper bound of full duplex network capacity is derived through disk-packing. Based on this result, the full duplex gain is studied in a wireless network. Due to asymptotic analysis, this result does not provide an explicit capacity gain but an upper bound of the gain.

To derive an explicit capacity gain of a full duplex wireless network over half duplex, transmission capacity is studied by leveraging the tools of *stochastic geometry* [13] in this paper. Transmission capacity is defined as the maximum throughput in an unit area, subject to a certain link rate and outage probability. For a half duplex wireless network, transmission capacity is derived in [14] where the network topology is modeled as a spatial point process. Due to full duplex communications on each radio in a full duplex wireless network, the network topology has to be modeled in a different way. In this paper, a Thomas cluster point process is used to model the network topology. More specifically, each cluster is represented by a virtual parent node, which follows the Poisson point process. Moreover, there are two daughter points scattering in each cluster with normal distribution. As a result, all daughter points form a Thomas cluster point process. Based on the Thomas cluster point process, the aggregate interference experienced by a

- *X. Wang is with the UM-SJTU Joint Institute, Shanghai Jiao Tong University, Shanghai, China. E-mail: wxudong@ieee.org.*
- *H. Huang is with the Signal Processing Department, Nanjing Research Institute of Electronics Technology, Nanjing 210039, China. E-mail: peterhuang1988@hotmail.com.*
- *T. Hwang is with the Department of Electrical and Electronic Engineering, Yonsei University, Seoul, Korea. E-mail: twhwang@yonsei.ac.kr.*

Manuscript received 2 Jan. 2015; revised 6 Oct. 2015; accepted 10 Oct. 2015. Date of publication 19 Oct. 2015; date of current version 2 Aug. 2016.
For information on obtaining reprints of this article, please send e-mail to: reprints@ieee.org, and reference the Digital Object Identifier below.
Digital Object Identifier no. 10.1109/TMC.2015.2492544

typical full duplex link is derived following a modified Palm theory. Moreover, the statistical distribution function [15] and the tail probability [16] of the aggregate interference are analyzed. Our analysis show that under the same network density the aggregate interference of a full duplex wireless network is more dispersed than that of a half duplex wireless network. Based on the aggregate interference, the transmission capacity is then derived for a full duplex wireless network where the MAC protocol follows slotted ALOHA. It should be noted that two full duplex transmission modes [11] exist in a wireless network, i.e., full duplex relay (FDR) mode (or called asymmetrical full duplex communications) and bi-directional exchange (BDE) mode (or called symmetrical full duplex communications). However, for capacity analysis, since all nodes in the network are assumed to have full duplex capability and work in saturation mode, two communication nodes can always form a full duplex link in the BDE mode. Thus, only BDE mode is considered in this paper.

Recently the research results reported in [17], [18] are closely related to our work. In [17] the achievable throughput is characterized by comparing throughput regions between MIMO, full-duplex, and their variants. Precise conditions under which the throughput gain is achieved are derived. Two major differences exist between the work in [17] and our paper. First, the analysis in [17] is based on a binary interference model, but our work considers SINR interference model so that the relationship between capacity again and physical layer parameters can be studied. Second, in [17] throughput gain is studied by comparing different optimal throughput regions of full duplex communication networks, MIMO networks, and their variants. In our paper, an exact result is derived for the capacity gain achieved by a full duplex network over a half duplex network. In [18] spatial-average throughput gain is derived via stochastic geometry for a full duplex wireless network. However, as pointed out in [18], it is non-trivial to apply the classical stochastic geometry model to a full duplex network. Thus, the derivation in [18] is based on a Poisson-bipolar model, so the receivers in the network do not actually belong to the Poisson point process of network nodes. Moreover, the closed-form results are derived by assuming fixed link distance; for random link distance, the results are confirmed through simulations.

The main contributions of our paper are summarized as follows. We leverage the Thomas cluster point process to model the network nodes in a full duplex wireless network. Based on the Thomas cluster point process, a new aggregate interference model is developed, and the property of the tail distribution of aggregate interference is investigated. The transmission capacity of a full duplex wireless network is then derived based on this interference model and a slotted ALOHA MAC protocol. Comparisons of transmission capacity between half duplex and full duplex networks are conducted, which reveals the limitations of full duplex communications in a large scale wireless network.

The rest of this paper is organized as follows. System models are described in Section 2. The new aggregate interference model is derived and the independency of aggregate interference on the typical full duplex links is presented in Section 3, where new aggregate interference model's relation to the aggregate interference of a half duplex wireless network is also analyzed. The distribution of aggregate interference for both half duplex and full duplex wireless networks are compared in Section 4. The transmission capacity is derived in Section 5. Numerical results are presented in Section 6, where limitations of a full duplex wireless network are revealed. Discussions on reasons for limited capacity gain from full duplex communications are conducted in Section 7. The paper is concluded in Section 8.

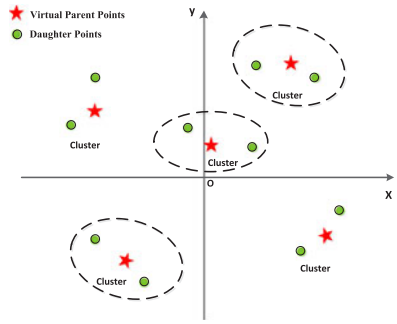

Fig. 1. Thomas cluster point process with two daughter points in each cluster.

2 System Model

2.1 Network Topology

When analyzing the network capacity via stochastic geometry [19], the network topology gives a distribution of active transmitters. For half duplex communications, the network topology usually follows a Poisson point process [20]. Considering a full duplex wireless network with the BDE mode, every two nodes are paired to achieve full duplex communications. This feature leads to a network topology with a clustering pattern. Thus, a Thomas cluster point process [13] on a two-dimensional plane is adopted as the network topology model. It is constructed by homogeneous independent clustering upon a parent point process. The parent point process $\Phi_p = \{\mathbf{x}_1, \mathbf{x}_2, \ldots\}$ is a stationary Poisson process with intensity λ_p, as shown by five-pointed stars in Fig. 1. The clusters are of the form $C^{\mathbf{x}_i} = C_i + \mathbf{x}_i = \{\mathbf{x} + \mathbf{x}_i : \mathbf{x} \in C_i\}$ for each $\mathbf{x}_i \in \Phi_p$. The $\{C_i\}$ are a family of independent identically distributed finite point sets. In this paper, two daughter points are assumed to be in each cluster C_i and represent a pair of full duplex communication nodes. These two points are scattered independently and identically following a normal distribution $f(\mathbf{x})$ around the parent point. This normal distribution $f(\mathbf{x})$ has a mean of $(0, 0)$ and a variance matrix of $\begin{pmatrix} \sigma^2 & 0 \\ 0 & \sigma^2 \end{pmatrix}$ and is given as follows:

$$f(\mathbf{x}) = \frac{1}{2\pi\sigma^2} \exp\left(-\frac{\|\mathbf{x}\|^2}{2\sigma^2}\right). \tag{1}$$

An example of such a distribution is shown in Fig. 1, where green circles depict the daughter points in a cluster. Note that the Thomas cluster process only includes daughter points while parent points just indicate a virtual point process. Hence, a Thomas cluster point process can be represented by

$$\Phi = \bigcup_{\mathbf{x}\in\Phi_p} C^{\mathbf{x}}. \quad (2)$$

Since the point process in this paper follows a different model than that used in existing analytical work for half duplex network, we use the concept of *network density* to avoid inconsistency of node density between half duplex and full duplex networks. In a half duplex network, a Poisson point process with intensity λ_p depicts the transmitting nodes. Due to half duplex communications, the total number of nodes in the network actually has an intensity of $2\lambda_p$. In a full duplex network formed by a Thomas cluster process, if parent nodes follow a Poisson point process with intensity λ_p and each cluster holds two daughter nodes, then the total number of nodes in the network has an intensity of $2\lambda_p$. Thus, for both half duplex and full duplex networks, we define λ_p as the *network density* of both networks. Thus, given the same λ_p, the actual node density in both networks is the same, i.e., λ_p.

2.2 Physical Layer Settings

Assume all nodes transmit with the same power P, and the transmission bandwidth is B, while the background noise is Gaussian with power spectrum density N_0. Hence, the received noise power is BN_0. To model signal propagation through a wireless channel, two types of fading are considered: small-scale fading and large-scale fading. In this paper, small scale fading is captured by Rayleigh channel fading with unit mean, while large-scale fading is represented by a path attenuation model. If a transmitter X at location $\mathbf{x}$ tries to send signals to a receiver Y at location $\mathbf{y}$, then the received power at Y is $P \cdot h_{XY} \cdot g(\mathbf{y}-\mathbf{x})$, where h_{XY} is the power fading coefficient associated with the wireless channel between nodes X and Y, and $g(\mathbf{x}) : \mathbb{R}^2 \rightarrow \mathbb{R}^+$ is the path-loss function, representing the path attenuation model. We choose the commonly used path-loss functions $\|\mathbf{x}\|^{-\alpha}$ with $\alpha > 2$, which is normalized without loss of generalization. The selected path-loss model is commonly used in existing analytical work based on stochastic geometry, but it is not appropriate for near-field communications. Fortunately, it is applicable to most practical wireless networks such as wireless mesh networks.

2.3 Distance of the Typical Link

To derive transmission capacity of a wireless network, we need to focus on one link in the wireless network, which is called a *typical link*. The transmission rate of the typical link is determined by its signal-to-interference-noise ratio (SINR), and the interference is the aggregate interference from concurrent transmissions from other links. To derive the interference, the link distance is a key parameter.

In the network topology following the previously-defined Thomas cluster point process, link distance d_l is the distance between the two points in the cluster. We know that these two points (i.e., $\mathbf{x}_1$ and $\mathbf{x}_2$) are distributed identically with a two-dimensional normal distribution $f(\mathbf{x})$ of zero mean and variance $\begin{pmatrix}\sigma^2 & 0\\ 0 & \sigma^2\end{pmatrix}$ around the virtual parent node $\mathbf{z}_0$. In other words, $(\mathbf{x}_2-\mathbf{z}_0)$ and $(\mathbf{x}_1-\mathbf{z}_0)$ are two-dimensional Gaussian random vectors. Subtracting $(\mathbf{x}_2-\mathbf{z}_0)$ from $(\mathbf{x}_1-\mathbf{z}_0)$, vector $(\mathbf{x}_2-\mathbf{x}_1)$ is obtained. It can be concluded that vector $(\mathbf{x}_2-\mathbf{x}_1)$ is also a Gaussian random vector with mean $(0,0)$ and variance matrix $\begin{pmatrix}2\sigma^2 & 0\\ 0 & 2\sigma^2\end{pmatrix}$. Thus, the link distance $d_l = \|\mathbf{x}_2-\mathbf{x}_1\|$ is Rayleigh random variable with parameter $\sqrt{2}\sigma$:

$$f_{d_l}(t) = \frac{t}{2\sigma^2} e^{-\frac{t}{4\sigma^2}}. \quad (3)$$

2.4 Medium Access Control

To evaluate transmission capacity, we assume that every node always has packets for its paired target receiver. A slotted ALOHA is considered as the MAC protocol, and link transmissions are active with medium access probability p.

In full duplex communications, the two nodes in one cluster can communicate with each other simultaneously in the same frequency. To make full use of full duplex communications, the paired nodes are assumed to start transmission simultaneously. In any time slot, all the potential transmitters forms a Thomas cluster point process with two daughter points in each cluster. Thus, the transmitter density becomes $2\lambda_p$, where λ_p is the network density, as defined before.

For comparison, a slotted ALOHA protocol is adopted for half duplex communications in the same network topology of the Thomas cluster point process. More specifically, if the radio of a node is half duplex, at most one transmission between the paired nodes is permitted in the cluster. In other words, time division duplex (TDD) is used to support bidirectional communications in the cluster, and the paired nodes in the cluster take turns to be the potential transmitter in one slot. Thus, the transmitter density is λ_p if nodes in a cluster are half duplex radios. This density is the same as that in a half duplex network following a Poisson point process with an intensity λ_p.

3 Aggregate Interference

To understand the aggregate interference of a typical link, we first need to consider the effect of MAC on network topology.

Under a slotted ALOHA protocol, the active transmitters form a new point process. Consider the Poisson point process with density λ in a half duplex wireless network. According to independent thinning theorem [13], a slotted ALOHA with medium access probability p results in that the active transmitters form a Poisson point process with density $p\lambda$. In a full duplex wireless network, the virtual parent points with density λ are thinned independently under a slotted ALOHA with medium access probability p. Similar to a half duplex wireless network, the active parent points form a Poisson point process with density $p\lambda$. Considering the relation between a virtual parent node and its two daughter points of a full duplex link, we know the active daughter points also form a Thomas cluster point process with density of $2p\lambda_p$.

Since the aggregate interference is viewed from the receiver of a typical link, the interference components are from all the active wireless nodes but the transmitter of the typical link. Thus, viewed from a typical receiver, the

distribution of nodes, which is also called the reduced Palm distribution, needs to be determined. The reduced Palm distribution is the conditional distribution of all points but the typical point under the condition that there is a point of the point process at a given location. In a half duplex wireless network following a Poisson point process, the Slivnyak's Theorem [13] concludes that the reduced Palm distribution of a Poisson point process is also a Poisson point process with the same density. Thus, from the perspective of a typical receiver, all the transmitters that generate interference to the typical link also form a Poisson point process with the same density.

In a network topology with a Thomas cluster point process, all wireless nodes are transmitters and receivers at the same time for full duplex communications. Therefore, every active link's receiver is also a transmitter, making aggregate interference on the typical link become inter-cluster aggregate interference. The Slivnyak's Theorem does not help derive the distribution of inter-cluster interferers. In this section, this problem is solved via a unique construction of the Thomas cluster process as well as the Slivnyak's Theorem.

3.1 Inter-Cluster Aggregate Interference in Full Duplex Communications

With a slotted ALOHA protocol, all active transmitters form a Thomas cluster Point process Φ' with density $2p\lambda_p$. Since the Thomas cluster point process is stationary, one transmitter[1] of a typical link can be assumed to be located at the origin $\mathbf{o}$ of the plane. We denote the typical cluster as ϕ_o, which contains the typical link.

The location of the virtual parent point in the typical cluster ϕ_o is denoted as $\mathbf{z}_p$, while location of the paired typical receiver is denoted as $\mathbf{z}$. Thus, the typical link distance is $d = \|\mathbf{z}\|$. The aggregate interference $I(\mathbf{z})$ on the typical receiver is the inter-cluster aggregate interference, given by

$$I(\mathbf{z}) = \sum_{\mathbf{x}\in\Phi'\setminus\{\phi_o\}} P \cdot h_X \cdot g(\mathbf{x}-\mathbf{z}), \tag{4}$$

where P is the transmitting power, h_X is the power fading coefficient associated with the wireless channel between nodes X and Z, and $g(\mathbf{x})$ is the path-loss function, representing the path attenuation model.

Note that the virtual parent process of the Thomas cluster process Φ', denoted by Φ'_p, is a Poisson Point process. According to the Slivnyak's Theorem, as viewed from the typical parent point $\mathbf{z}_p$, all the other parent points in Φ'_p form a Poisson point process with density $p\lambda_p$. Moreover, the Poisson point process Φ'_p is stationary [21], which means the new point process $\Phi'_{p\mathbf{z}} = \{\mathbf{x}+\mathbf{z} : \mathbf{x} \in \Phi'_p\}$ generated by parallel translation of fixed vector $\mathbf{z}$ is also a Poisson point process with density $p\lambda_p$ on the plane.

Viewed from the typical receiver $\mathbf{z}$, the point process Φ'_p is parallel translated into a new point process $\Phi'_{p\mathbf{z}} = \{\mathbf{x}+\mathbf{z} : \mathbf{x} \in \Phi'_p\}$. Due to independent scattering of daughter points in the cluster, the vector $\mathbf{z}$ is a random vector independent of Φ'_p. Thus, conditional on the vector $\mathbf{z}$, the parallel translated point process $\Phi'_{p\mathbf{z}}$ is Poisson point process, making all daughter points in the other clusters form a Thomas cluster point process with density $2p\lambda_p$. It can be concluded that all daughter points in the other clusters form a Thomas cluster point process with density $2p\lambda_p$ under all the samples of vector $\mathbf{z}$ when treating the $\mathbf{z}$ as a random vector. As a result, viewed from the typical receiver $\mathbf{z}$, all daughter points in the other clusters also form a Thomas cluster process with the density $2p\lambda_p$.

Thus, the aggregate interference experienced by the receiver of the typical link is equal to the interference from all the daughter points in the Thomas cluster point process. Therefore,

$$I(\mathbf{z}) = \sum_{\mathbf{x}\in\Phi'\setminus\{\phi_o\}} P \cdot h_X \cdot g(\mathbf{x}-\mathbf{z}) = \sum_{\mathbf{x}\in\Phi'} P \cdot h_X \cdot g(\mathbf{x}). \tag{5}$$

Based on the inter-cluster aggregate interference model, the mean and variance of the inter-cluster interference are derived as follows.

Theorem 1. *Let $\Phi \subset \mathbb{R}^2$ be a Thomas cluster Point Process with two daughter points in each cluster, which is the network topology of a full duplex wireless network. Assume the node density of the parent process (i.e., the network density) is λ_p. Considering slotted ALOHA as the MAC protocol with access probability p, the mean and variance of the inter-cluster interference on the typical link are given as follows:*

$$\begin{cases} \mathbb{E}[I(\mathbf{z})] = 2p\lambda_p P \int_{\mathbb{R}^2} g(\mathbf{s}) d\mathbf{s}. \\ var[I(\mathbf{z})] = 2p\lambda_p P^2 [\int_{\mathbb{R}^2} g^2(\mathbf{s}) d\mathbf{s} + K], \end{cases} \tag{6}$$

where $K = \int_{\mathbb{R}^4} g(\mathbf{s}) g(\mathbf{s}+\mathbf{y}) f(\mathbf{y}) d\mathbf{y} d\mathbf{s}$.

Proof. See Appendix A, which can be found on the Computer Society Digital Library at http://doi.ieeecomputersociety.org/10.1109/TMC.2015.2492544. □

3.2 Spatial Correlation of Aggregate Interference

Under full duplex communications, wireless nodes are transmitters and receivers simultaneously. In our Thomas cluster point process model, two nodes lie in one cluster and form a full duplex link. The aggregate interference on both nodes are from active transmissions in other clusters. It is necessary to determine the spatial correlation of aggregate interference on both nodes when calculate the network capacity. Suppose that the parent node of typical cluster lies in the origin $\mathbf{o}$, and the two daughter points $\mathbf{z}_1$ and $\mathbf{z}_2$ lie in position $\mathbf{u}$ and point $\mathbf{v}$. Note that, from the view of typical parent points, all the daughter points in other cluster follow Thomas cluster point process with the same density. Thus, the aggregate interference $I(\mathbf{u})$ on $\mathbf{z}_1$ and the aggregate interference $I(\mathbf{v})$ on $\mathbf{z}_2$ are shown as follows:

$$\begin{cases} I(\mathbf{u}) = \sum_{\mathbf{x}\in\Phi'} P \cdot h_{\mathbf{x}u} \cdot g(\mathbf{x}-\mathbf{u}), \\ I(\mathbf{v}) = \sum_{\mathbf{x}\in\Phi'} P \cdot h_{\mathbf{x}v} \cdot g(\mathbf{x}-\mathbf{v}), \end{cases} \tag{7}$$

where P is the transmission power, $h_{\mathbf{x}u}$ the power fading coefficient associated with the wireless channel between nodes $\mathbf{x}$ and $\mathbf{z}_1$, and $h_{\mathbf{x}v}$ is the power fading coefficient associated with the wireless channel between nodes $\mathbf{x}$ and $\mathbf{z}_2$.

1. There are a pair of transmitters in a typical link, but the other transmitter can be treated in the same way.

Moreover, $g(\mathbf{x})$ is the path-loss function, representing the path attenuation model. From Theorem 1 and identical distribution property, we can get the mean and the variance of aggregate interference $I(\mathbf{z}_1)$ and $I(\mathbf{z}_2)$

$$\begin{cases} \mathbb{E}[I(\mathbf{u})] = \mathbb{E}[I(\mathbf{v})] = 2p\lambda_p P \int_{\mathbb{R}^2} g(\mathbf{s})d\mathbf{s}, \\ var[I(\mathbf{u})] = var[I(\mathbf{v})] = 2p\lambda_p P^2[\int_{\mathbb{R}^2} g^2(\mathbf{s})d\mathbf{s} + K], \end{cases} \tag{8}$$

where $K = \int_{\mathbb{R}^4} g(\mathbf{s})g(\mathbf{s}+\mathbf{y})f(\mathbf{y})d\mathbf{y}d\mathbf{s}$. The mean product of the aggregate interference $I(\mathbf{u})$ and $I(\mathbf{v})$ is given by

$$\begin{aligned} \mathbb{E}[I(\mathbf{u})I(\mathbf{v})] &= P^2\mathbb{E}\left[\sum_{\mathbf{x}\in\Phi'} h_{\mathbf{x}u}g(\mathbf{x}-\mathbf{u})\sum_{\mathbf{y}\in\Phi'} h_{\mathbf{x}v}g(\mathbf{y}-\mathbf{v})\right] \\ &= 2P^2p\lambda_p\int_{\mathbb{R}^2} g(\mathbf{s}-\mathbf{u})g(\mathbf{s}-\mathbf{v})d\mathbf{s} + \left[2Pp\lambda_p\int_{\mathbb{R}^2} g(\mathbf{s})d\mathbf{s}\right]^2 \\ &\quad + 2P^2p\lambda_p K(\mathbf{u},\mathbf{v}), \end{aligned} \tag{9}$$

where

$$K(\mathbf{u},\mathbf{v}) = \int_{\mathbb{R}^4} g(\mathbf{s}-\mathbf{u})g(\mathbf{s}-\mathbf{v}+\mathbf{y})f(\mathbf{y})d\mathbf{y}d\mathbf{s}.$$

The above derivation is given in Appendix B, available online.

Theorem 2. *Spatial correlation of aggregate interference $I(\mathbf{z}_1)$ and $I(\mathbf{z}_2)$ is given by*

$$\zeta(\mathbf{u},\mathbf{v}) = \frac{\int_{\mathbb{R}^2} g(\mathbf{s}-\mathbf{u})g(\mathbf{s}-\mathbf{v})d\mathbf{s} + K(\mathbf{u},\mathbf{v})}{\int_{\mathbb{R}^2} g^2(\mathbf{s})d\mathbf{s} + K}, \tag{10}$$

where $K = \int_{\mathbb{R}^4} g(\mathbf{s})g(\mathbf{s}+\mathbf{y})f(\mathbf{y})d\mathbf{y}d\mathbf{s}$ and

$$K(\mathbf{u},\mathbf{v}) = \int_{\mathbb{R}^4} g(\mathbf{s}-\mathbf{u})g(\mathbf{s}-\mathbf{v}+\mathbf{y})f(\mathbf{y})d\mathbf{y}d\mathbf{s}.$$

Moreover, $\zeta(\mathbf{u},\mathbf{v}) = 0$ when $\mathbf{u} \neq \mathbf{v}$.

Proof. The result is obtained by definition of correlation,

$$\zeta(u,v) = \frac{\mathbb{E}[I(\mathbf{z}_1)I(\mathbf{z}_2)] - \mathbb{E}[I(\mathbf{z}_1)]^2}{var[I(\mathbf{z}_1)]}. \tag{11}$$

Moreover, due to basic knowledge of inequality

$$\frac{x+y}{a+b} \leq \frac{x+y}{a}$$

when all parameters are positive, we can get that

$$0 \leq \zeta(u,v) \leq \frac{\int_{\mathbb{R}^2} g(\mathbf{s}-\mathbf{u})g(\mathbf{s}-\mathbf{v})d\mathbf{s} + K(\mathbf{u},\mathbf{v})}{\int_{\mathbb{R}^2} g^2(\mathbf{s})d\mathbf{s}}. \tag{12}$$

When $\mathbf{u} \neq \mathbf{v}$, we can make following conclusion by the proof of [22, Corollary 3]:

$$\frac{\int_{\mathbb{R}^2} g(\mathbf{s}-\mathbf{u})g(\mathbf{s}-\mathbf{v})d\mathbf{s}}{\int_{\mathbb{R}^2} g^2(\mathbf{s})d\mathbf{s}} = 0. \tag{13}$$

As for the second term in Eq. (12), it is derived with the following results:

$$\begin{aligned} \frac{K(\mathbf{u},\mathbf{v})}{\int_{\mathbb{R}^2} g^2(\mathbf{s})d\mathbf{s}} &= \frac{\int_{\mathbb{R}^4} g(\mathbf{s}-\mathbf{u})g(\mathbf{s}-\mathbf{v}+\mathbf{y})f(\mathbf{y})d\mathbf{y}d\mathbf{s}}{\int_{\mathbb{R}^2} g^2(\mathbf{s})d\mathbf{s}} \\ &= \int_{\mathbb{R}^2}\left[\frac{\int_{\mathbb{R}^2} g(\mathbf{s}-\mathbf{u})g(\mathbf{s}-\mathbf{v}+\mathbf{y})d\mathbf{s}}{\int_{\mathbb{R}^2} g^2(\mathbf{s})d\mathbf{s}}\right] f(\mathbf{y})d\mathbf{y}. \end{aligned} \tag{14}$$

Based on Eq. (13), we can conclude that

$$\frac{\int_{\mathbb{R}^2} g(\mathbf{s}-\mathbf{u})g(\mathbf{s}-\mathbf{v}+\mathbf{y})d\mathbf{s}}{\int_{\mathbb{R}^2} g^2(\mathbf{s})d\mathbf{s}} = \mathbf{1}_{(\mathbf{v}-\mathbf{u})}(\mathbf{y}), \tag{15}$$

where $\mathbf{1}_{(\mathbf{v}-\mathbf{u})}(\mathbf{y}) = 1$ if $\mathbf{y} = \mathbf{v}-\mathbf{u}$, and $\mathbf{1}_{(\mathbf{v}-\mathbf{u})}(\mathbf{y}) = 0$ for other values of $\mathbf{y}$. Then,

$$\begin{aligned} \frac{K(\mathbf{u},\mathbf{v})}{\int_{\mathbb{R}^2} g^2(\mathbf{s})d\mathbf{s}} &= \int_{\mathbb{R}^2}\left[\frac{\int_{\mathbb{R}^2} g(\mathbf{s}-\mathbf{u})g(\mathbf{s}-\mathbf{v}+\mathbf{y})d\mathbf{s}}{\int_{\mathbb{R}^2} g^2(\mathbf{s})d\mathbf{s}}\right] f(\mathbf{y})d\mathbf{y} \\ &= \int_{\mathbb{R}^2} \mathbf{1}_{(\mathbf{v}-\mathbf{u})}(\mathbf{y})f(\mathbf{y})d\mathbf{y} \\ &= 0. \end{aligned} \tag{16}$$

So $\zeta(\mathbf{u},\mathbf{v}) = 0$ when $\mathbf{u} \neq \mathbf{v}$. □

Based on this theorem, we can conclude that the correlation of aggregate interference $I(\mathbf{z}_1)$ and $I(\mathbf{z}_2)$ is zero for our model, in which the daughter points in the typical cluster do not lie in the same points, i.e., $\mathbf{u} \neq \mathbf{v}$. Combining with independent channel model, it is concluded that the full duplex link transmissions are independent at the same communication slot in the full duplex wireless network. This result can also be explained by the following two properties of two daughter points at locations u and v: 1) Interference between these two daughter points can be neglected, because perfect self-interference cancellation is assumed in a full duplex radio; 2) The two daughter points are located independently and each can be considered as a typical node, so their experienced interference from other nodes is independent from each other. Thus, their interference has zero correlation. It should be noted that these two properties rely on an implicit condition, i.e., the nodes at locations u and v cannot be so close to each other as the case in near-field communications. This condition is satisfied in our paper, because the path-loss model $g(\mathbf{x}) = \frac{1}{\|\mathbf{x}\|^\alpha}$ is selected. This model is actually meaningful for most multihop wireless networks such as wireless mesh networks. Following this model, the main contributor to the interference is the the the nearest transmitter. For two nodes at u and v, as long as $u \neq v$, there exist small $\delta > 0$, such that the disc $B(u,\delta)$ and the disc $B(v,\delta)$ do not intersect each other. The transmitters in these two discs make main contributions to the aggregate interference on its center node u and v, respectively. Moreover, transmitters in the disc $B(u,\delta)$ and the disc $B(v,\delta)$ are independent in a Thomas cluster point process, which leads to zero correlation between the interference at locations u and v. A similar case has been observed and discussed in a half duplex network in [22].

3.3 Equivalent Model of Half Duplex Communication

We apply the above Thomas cluster process to a half duplex wireless network with TDD. As stated in the following theorem, the network point process is equivalent to a Poisson

point process with the same network density. This result confirms that our analytical framework based on a Thomas cluster process is consistent with a traditional Poisson point process model in a half duplex wireless network, which indicates the effectiveness of our analysis for a full duplex wireless network.

Theorem 3. *Let Φ_1 be a Thomas cluster process with one transmitting point in each cluster, the density of virtual parent point process of Φ_1 be λ_p, and Φ_2 be a Poisson point process with density λ_p. Then, Φ_1 and Φ_2 have the same spatial distribution.*

Proof. In the Thomas cluster process Φ_1, the virtual parent point process is a Poisson point process with density λ_p, and the daughter point is placed around its virtual parent point with the normal distribution. Moreover, the distribution function, as shown in Eq. (1), only depends on $(\mathbf{y}-\mathbf{x})$. According to the displacement theorem [23], by treating the virtual parent point process as the original process and the daughter point process as the displaced point process, then we know that the displaced point process is also Poisson with the same density. Thus, the Thomas cluster process Φ_1 is also a Poisson point process with the same density. Thus, Φ_1 and Φ_2 have the same spatial distribution, which means the two processes are equivalent. □

In Section 5.1, we will further study the equivalence of two models by comparing the successful transmission probability in a half duplex network.

4 Tail Probability of Aggregate Interference

To investigate the distribution of aggregate interference on a typical link, we derive the asymptotic tail probability, i.e., the complementary cumulative distribution function (CCDF) of aggregate interference $I(\mathbf{z})$, represented by $\bar{F}_I(y)=\mathbb{P}(I(\mathbf{z})\geq y)$ when $y\to\infty$. The derivations are conducted based on a theorem in [16]. This theorem provides the bounds for the tail probability of aggregate interference when all nodes follow a general spatial point process [16]. It is summarized as follows.

Theorem 4. *Let $\Phi\subset\mathbb{R}^2$ be a stationary spatial point process. Assume that all points in the process contribute to the interference on a typical link, represented by $I(\mathbf{z})$. The tail probability $F_I(y)$ of $I(\mathbf{z})$ is lower bounded by $\bar{F}_I^l(y)$ and upper bounded by $\bar{F}_I^u(y)$, and*

$$\begin{cases}\bar{F}_I^l(y)=1-\mathcal{G}(F_h(\frac{y}{g(\cdot)}))\\ \bar{F}_I^u(y)=1-(1-\varphi(y))\mathcal{G}(F_h(\frac{y}{g(\cdot)})),\end{cases}\tag{17}$$

where $F_h(\cdot)$ denotes the CDF of the power fading coefficient h, and $\mathcal{G}(l(\cdot))$ is the generating function of function $l(\mathbf{x})$, which is defined as $\mathcal{G}(l(\cdot))=\mathbb{E}[\prod_{\mathbf{x}\in\Phi}l(\mathbf{x})]$. Moreover, $\varphi(y)$ is given as

$$\varphi(y)=\frac{1}{y}\mathbb{E}\sum_{\mathbf{x}\in\Phi}g(\mathbf{x})\int_0^{y/g(\mathbf{x})}vdF_h(v).\tag{18}$$

To obtain the lower and upper bounds of tail probability of the aggregate interference in half duplex and full duplex wireless networks, we only need to restrict the general point process to Poisson point process with density $p\lambda_p$ and Thomas cluster point process with density $2p\lambda_p$. For these two processes, the generating function of $F_h(\frac{y}{g(\mathbf{x})})$ (i.e., $\mathcal{G}(F_h(\frac{y}{g(\cdot)}))$) and the function $\varphi(y)$ are summarized in the following lemma.

Lemma 5. *For Poisson point process with density $p\lambda_p$, the generating function of $F_h(\frac{y}{g(\mathbf{x})})$ (i.e., $\mathcal{G}^H(F_h(\frac{y}{g(\cdot)}))$) and the function $\varphi^H(y)$ are derived as follows:*

$$\begin{cases}\mathcal{G}^H(F_h(\frac{y}{g(\cdot)}))=e^{-p\lambda_p\int_{\mathbb{R}^2}(1-F_h(\frac{y}{g(\mathbf{x})}))d\mathbf{x}},\\ \varphi^H(y)=\frac{1}{y}p\lambda_p\int_{\mathbb{R}^2}g(\mathbf{x})\int_0^{y/g(\mathbf{x})}vdF_h(v)d\mathbf{x}.\end{cases}\tag{19}$$

For Thomas cluster point process with density $2p\lambda_p$, the generating function of $F_h(\frac{y}{g(\mathbf{x})})$ (i.e., $\mathcal{G}^F(F_h(\frac{y}{g(\cdot)}))$) and the function $\varphi^F(y)$ are derived as follows:

$$\begin{cases}\mathcal{G}^F(F_h(\frac{y}{g(\cdot)}))=e^{-p\lambda_p\int_{\mathbb{R}^2}[1-(\int_{\mathbb{R}^2}F_h(\frac{y}{g(\mathbf{x}+\mathbf{z})})f(\mathbf{z})d\mathbf{z})^2]d\mathbf{x}},\\ \varphi^F(y)=\frac{1}{y}2p\lambda_p\int_{\mathbb{R}^2}g(\mathbf{x})\int_0^{y/g(\mathbf{x})}vdF_h(v)d\mathbf{x}.\end{cases}\tag{20}$$

Proof. In a Poisson point process Φ with intensity λ, the generating function of function $l(\mathbf{x})$ is $\mathcal{G}(l(\cdot))=\mathbb{E}\big(\prod_{\mathbf{x}\in\Phi}l(\mathbf{x})\big)=e^{-\lambda\int_{\mathbb{R}^2}(1-l(\mathbf{x}))d\mathbf{x}}$ [23]. Moreover, considering function $q(\mathbf{x})$, its mean sum over Φ is $\mathbb{E}\big(\sum_{\mathbf{x}\in\Phi}q(\mathbf{x})\big)=\lambda\int_{\mathbb{R}^2}q(\mathbf{x})d\mathbf{x}$ [23]. Let $l(\mathbf{x})=F_h(\frac{y}{g(\mathbf{x})})$, $q(\mathbf{x})=g(\mathbf{x})\int_0^{y/g(\mathbf{x})}vdF_h(v)$, and $\lambda=p\lambda_p$, the results in 19 are obtained.

As for a Thomas cluster process Φ_1 with the intensity λ, the generating function of $l(\mathbf{x})$ is [16]:

$$\begin{aligned}\mathcal{G}_{\Phi_1}(l(\mathbf{x}))&=\mathbb{E}\left(\prod_{\mathbf{x}\in\Phi_1}l(\mathbf{x})\right)\\&=\exp\left(-\lambda\int_{\mathbb{R}^2}\left[1-M\left(\int_{\mathbb{R}^2}l(\mathbf{x}+\mathbf{y})f(\mathbf{y})d\mathbf{y}\right)\right]d\mathbf{x}\right),\end{aligned}$$

where $M(n)=\sum_{i=0}^{\infty}p_in^i$ is the moment generating function of the number of points in the typical cluster. In this paper, there are two fixed points in the cluster, so $M(n)=n^2$. Thus,

$$\mathcal{G}_{\Phi_1}(l(\mathbf{x}))=\exp\left(-\lambda\int_{\mathbb{R}^2}\left[1-\left(\int_{\mathbb{R}^2}l(\mathbf{x}+\mathbf{y})f(\mathbf{y})d\mathbf{y}\right)^2\right]d\mathbf{x}\right).\tag{21}$$

Considering the same Thomas cluster process with two daughter points in each cluster, the mean sum of $q(\mathbf{x})$ over Φ_1 is

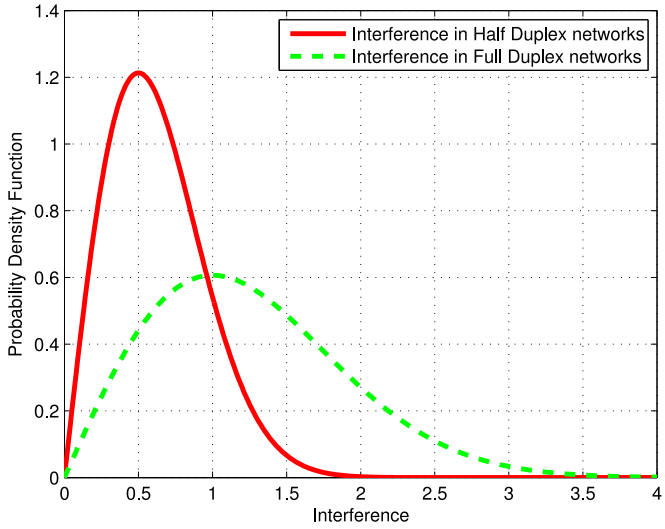

Fig. 2. A qualitative illustration of aggregate interference distribution in both networks.

$$\mathbb{E}\left(\sum_{\mathbf{x}\in\Phi_1} q(\mathbf{x})\right) = \mathbb{E}\left[\sum_{\mathbf{y}\in\Phi_p}\left(\sum_{\mathbf{s}\in N_0}^{\mathbf{x}=\mathbf{y}+\mathbf{s}} q(\mathbf{x})\right)\right] = 2\lambda\int_{\mathbb{R}^2}\int_{\mathbb{R}^2} q(\mathbf{s}+\mathbf{y})f(\mathbf{y})d\mathbf{y}d\mathbf{s} = 2\lambda\int_{\mathbb{R}^2} q(\mathbf{s})d\mathbf{s}. \tag{22}$$

Let $l(\mathbf{x}) = F_h(\frac{y}{g(\mathbf{x})})$, $q(\mathbf{x}) = g(\mathbf{x})\int_0^{y/g(\mathbf{x})} vdF_h(v)$, and $\lambda = p\lambda_p$, then the results in 20 are obtained. □

Based on Lemma 5, when y approaches infinity, the lower and upper bounds of the tail probability of the aggregate interference in half duplex and full duplex networks are summarized in following theorem.

Theorem 6. *Given $g(x) = \frac{1}{\|x\|^{\alpha}}$, the lower and upper bounds of CCDF $\bar{F}_I(y)$ of the aggregate interference in full duplex and half duplex networks scale in the following way as $y \to \infty$:*

$$\begin{cases} \bar{F}_I^{lH}(y) \sim \pi p\lambda_p y^{-\frac{2}{\alpha}}\int_0^{\infty} t^{\frac{2}{\alpha}}dF_h(t) \\ \bar{F}_I^{uH}(y) \sim \frac{\alpha}{\alpha-2}\pi p\lambda_p y^{-\frac{2}{\alpha}}\int_0^{\infty} t^{\frac{2}{\alpha}}dF_h(t), \end{cases} \tag{23}$$

and

$$\begin{cases} \bar{F}_I^{lF}(y) \sim \pi p\lambda_p y^{-\frac{2}{\alpha}}\int_0^{\infty} t^{\frac{2}{\alpha}}dF_h(t) \\ \bar{F}_I^{uF}(y) \sim \frac{2\alpha}{\alpha-2}\pi p\lambda_p y^{-\frac{2}{\alpha}}\int_0^{\infty} t^{\frac{2}{\alpha}}dF_h(t). \end{cases} \tag{24}$$

Proof. See Appendix C, available online. □

Theorem 6 implies that, under the same network density, the lower bounds of tail probability of the aggregate interference in both networks are equal, but the upper bound of a full duplex network is twice as that of a half duplex network. Moreover, from the Theorem 1, the mean and the variance of the aggregate interference in a full duplex network are larger than those in half duplex networks. Thus, considering the same network density, we conclude that the distribution of the aggregate interference in a full duplex network is more disperse than that in a half duplex network. With Theorems 1 and 6, the probability density function (PDF) of the aggregate interference in both networks is depicted qualitatively in Fig. 2.

5 Successful Transmission Probability and Transmission Capacity

In this section, the successful transmission probability of the typical link is derived for both a half duplex and a full duplex wireless network. The transmission capacity in both networks is then derived based on the successful transmission probability.

5.1 Successful Transmission Probability

Successful transmission occurs if the received signal interference plus noise ratio (SINR) is large than a threshold T, which is determined according to a required transmission rate. Considering a transmission distance is d, the probability of successful transmission $\mathbb{P}_{suc}(\mathbf{z})$ is given by

$$\mathbb{P}_{suc}(d,T) = \mathbb{P}\left(\frac{P\cdot h\cdot g(d)}{BN_0 + I(\mathbf{z})} \geq T\right). \tag{25}$$

Since the interference is expected to be much larger than the noise, i.e., $I(\mathbf{z}) \gg BN_0$, we neglect the background noise. Under this condition, wireless network is interference-limited, since the aggregate interference is the only factor that determines the capacity of the typical link. Normalizing the aggregate interference by the transmission power P, so

$$I(\mathbf{z}) = \sum_{\mathbf{x}\in\Phi'} h_X\cdot g(\mathbf{x}), \tag{26}$$

where Φ' is a Thomas cluster process. Thus, the probability of successful transmission is

$$\mathbb{P}_{suc}(d,T) = \mathbb{P}\left(\frac{h\cdot g(d)}{I(\mathbf{z})} \geq T\right) = \mathbb{P}\left(h \geq \frac{TI(\mathbf{z})}{g(d)}\right) = \int_0^{\infty} e^{-sT/g(d)}d\mathbb{P}(I(\mathbf{z}) \leq s) = L_{I(\mathbf{z})}(s)|_{s=T/g(d)}, \tag{27}$$

where $L_X(s)$ is the Laplace transform function of random variable X, i.e., $L_X(s) = \mathbb{E}[e^{-sX}]$.

For a full duplex wireless network, successful transmission probability of the typical link is based on the Laplace function of inter-cluster aggregate interference $L_{I(\mathbf{z})}(s) = \mathbb{E}[e^{-sI(\mathbf{z})}]$. The Laplace function of inter-cluster aggregate interference is derived as follows:

$$L_I(s) = \mathbb{E}[e^{-sI(\mathbf{z})}] = \mathbb{E}\left[e^{-s\left(\sum_{\mathbf{x}\in\Phi'} h_X\cdot g(\mathbf{x})\right)}\right] = \mathbb{E}\left(\prod_{\mathbf{x}\in\Phi'} e^{-s\cdot h_X\cdot g(\mathbf{x})}\right) = \mathbb{E}_{\Phi'}\left(\prod_{\mathbf{x}\in\Phi'}\mathbb{E}_{h_X}[e^{-s\cdot h_X\cdot g(\mathbf{x})}]\right) = \mathbb{E}_{\Phi'}\left[\prod_{x\in\Phi'} v(s,\mathbf{x})\right], \tag{28}$$

where $v(s,x) = \mathbb{E}_{h_X}[e^{-s\cdot h_X\cdot g(\mathbf{x})}] = \frac{1}{1+sg(\mathbf{x})}$, due to Rayleigh channel fading. Thus, the Laplace function of inter-cluster aggregate interference is equal to generating function $\mathcal{G}_{\Phi'}(v)$ of $v(s,\mathbf{x})$, i.e., $\mathbb{E}_{\Phi'}\left[\prod_{\mathbf{x}\in\Phi'} v(s,\mathbf{x})\right]$. Considering Eq. (21) and $\lambda = p\lambda_p$, we have

$$\begin{aligned}\mathcal{G}_{\Phi'}(v) &= \mathbb{E}_{\Phi'}\left[\prod_{\mathbf{x}\in\Phi'} v(s,\mathbf{x})\right] \\ &= \exp\left(-p\lambda_p \int_{\mathbb{R}^2}\left[1-\left(\int_{\mathbb{R}^2}\frac{1}{1+sg(\mathbf{x}+\mathbf{y})}f(\mathbf{y})d\mathbf{y}\right)^2\right]d\mathbf{x}\right) \\ &= \exp\left(-p\lambda_p \int_{\mathbb{R}^2}\left[1-\left(\int_{\mathbb{R}^2}\frac{1}{1+sg(\mathbf{x}-\mathbf{y})}f(\mathbf{y})d\mathbf{y}\right)^2\right]d\mathbf{x}\right).\end{aligned} \tag{29}$$

The last equality holds because $f(-\mathbf{y}) = f(\mathbf{y})$.

Combining Eq. (27) and Eq. (29), the successful transmission probability of a full duplex network is

$$\begin{aligned}&\mathbb{P}_{suc}^{Full}(d,T) = L_{I(\mathbf{z})}(s)|_{s=T/g(d)} \\ &= \exp\left(-p\lambda_p \int_{\mathbb{R}^2}\left[1-\left(\int_{\mathbb{R}^2}\frac{1}{1+Tg(\mathbf{x}-\mathbf{y})/g(d)}f(\mathbf{y})d\mathbf{y}\right)^2\right]d\mathbf{x}\right) \\ &= \exp\left\{-p\lambda_p \int_{\mathbb{R}^2}\left[1-\beta^2(\mathbf{x};d,T)\right]d\mathbf{x}\right\},\end{aligned} \tag{30}$$

where $\beta(\mathbf{x};d,T) = \int_{\mathbb{R}^2}\frac{1}{1+Tg(\mathbf{x}-\mathbf{y})/g(d)}f(\mathbf{y})d\mathbf{y}$.

5.2 The Case of Half Duplex Communications

For half duplex communications with a network topology following a Thomas cluster process, slotted ALOHA is also considered as the MAC protocol. Thus, in any time slot, all transmitting nodes form a Thomas cluster process Φ_1 with only one transmitting node in each cluster. Following the similar derivation for full duplex communications, the successful transmission probability of a typical link is the Laplace function of inter-cluster aggregate interference $I_1(\mathbf{z})$. Hence, the successful transmission probability of the typical link in a half duplex network is given by

$$\begin{aligned}&\mathbb{P}_{suc}^{Half}(d,T) = L_{I_1(\mathbf{z})}(s)|_{s=T/g(d)} \\ &= \exp\left(-p\lambda_p \int_{\mathbb{R}^2}\left[1-\int_{\mathbb{R}^2}\frac{1}{1+Tg(\mathbf{x}-\mathbf{y})/g(d)}f(\mathbf{y})d\mathbf{y}\right]d\mathbf{x}\right) \\ &= \exp\left\{-p\lambda_p \int_{\mathbb{R}^2}[1-\beta(\mathbf{x};d,T)]d\mathbf{x}\right\}.\end{aligned} \tag{31}$$

Moreover,

$$\begin{aligned}&\int_{\mathbb{R}^2}[1-\beta(\mathbf{x};d,T)]d\mathbf{x} \\ &= \int_{\mathbb{R}^2}\left[1-\int_{\mathbb{R}^2}\frac{1}{1+Tg(\mathbf{x}-\mathbf{y})/g(d)}f(\mathbf{y})d\mathbf{y}\right]d\mathbf{x} \\ &= \int_{\mathbb{R}^2}\left[\int_{\mathbb{R}^2}f(\mathbf{y})d\mathbf{y}-\int_{\mathbb{R}^2}\frac{1}{1+Tg(\mathbf{x}-\mathbf{y})/g(d)}f(\mathbf{y})d\mathbf{y}\right]d\mathbf{x} \\ &= \int_{\mathbb{R}^2}\int_{\mathbb{R}^2}\left(1-\frac{1}{1+Tg(\mathbf{x}-\mathbf{y})/g(d)}\right)f(\mathbf{y})d\mathbf{y}d\mathbf{x} \\ &= \int_{\mathbb{R}^2}\int_{\mathbb{R}^2}\left(1-\frac{1}{1+Tg(\mathbf{x})/g(d)}\right)f(\mathbf{y})d\mathbf{x}d\mathbf{y} \\ &= \int_{\mathbb{R}^2}\left(1-\frac{1}{1+Tg(\mathbf{x})/g(d)}\right)d\mathbf{x}.\end{aligned} \tag{32}$$

By combining Eqs. (31) and (32), the successful transmission probability of a typical link in a half duplex network is

$$\mathbb{P}_{suc}^{Half}(d,T) = \exp\left(-p\lambda_p \int_{\mathbb{R}^2}\left(1-\frac{1}{1+Tg(\mathbf{x})/g(d)}\right)d\mathbf{x}\right). \tag{33}$$

Considering a Poisson point process with density $p\lambda_p$, successful transmission probability $\mathbb{P}_{suc}^{PPP}(d,T)$ of a typical link in a half duplex network is [14]

$$\begin{aligned}\mathbb{P}_{suc}^{PPP}(d,T) &= \exp\left\{p\lambda_p \int_{\mathbb{R}^2}\left[1-v(s,\mathbf{x})|_{s=T/g(z)}\right]d\mathbf{x}\right\} \\ &= \exp\left(-p\lambda_p \int_{\mathbb{R}^2}\left(1-\frac{1}{1+Tg(\mathbf{x})/g(d)}\right)d\mathbf{x}\right).\end{aligned} \tag{34}$$

Comparing Eq. (33) and Eq. (34), we know that $\mathbb{P}_{suc}^{Half}(d,T) = \mathbb{P}_{suc}^{PPP}(d,T)$. This consistency validates our analytical framework following a Thomas cluster process.

5.3 Full Duplex versus Half Duplex

To simplify the derivations later, we define two parameters for both half duplex and full duplex networks as follows:

$$\begin{cases}\alpha^H(d,T) &= \int_{\mathbb{R}^2}[1-\beta(\mathbf{x};d,T)]d\mathbf{x} \\ \alpha^F(d,T) &= \int_{\mathbb{R}^2}\left[1-\beta^2(\mathbf{x};d,T)\right]d\mathbf{x}.\end{cases} \tag{35}$$

The relationship of these two parameters is captured in the following lemma.

Lemma 7. $\alpha^H(d,T) \le \alpha^F(d,T) \le 2\alpha^H(d,T), \forall T,d \in \mathbb{R}^+$.

Proof. From the form of $\beta(\mathbf{x};d,T)$, we know that

$$\beta(\mathbf{x};d,T) \le 1, \forall \mathbf{y} \in \mathbb{R}^2, d \in \mathbb{R}^+.$$

Moreover,

$$1-\beta^2(d,\mathbf{x};T) = (1-\beta(d,\mathbf{x};T))(1+\beta(d,\mathbf{x};T)).$$

Thus, we know that

$$\alpha^H(d,T) \le \alpha^F(d,T) \le 2\alpha^H(d,T), \forall T,d \in \mathbb{R}^+. \qquad \square$$

5.4 Transmission Capacity

Transmission throughput (TH), which represents mean throughput in a unit network area, is defined as

$$TH(d,T) = \lambda \log(1+T)\mathbb{P}_{suc}(d,T),$$

where the transmission link density is λ, T is the SINR threshold, and $\mathbb{P}_{suc}(d,T)$ is the successful transmission probability for the typical link with distance d. $\mathbb{P}_{suc}(d,T)$ is given by Eq. (30) and Eq. (31), respectively, for full duplex communications and half duplex communications. In this paper, the transmission link density is $p\lambda_p$ for a half duplex network. As discussed in Section 3, the transmission link density for a full duplex network is $2p\lambda_p$. However, both networks have the same node density λ_p.

Transmission capacity is defined as the maximum transmission throughput, subject to a constraint on the transmission outage probability of the typical link. Let ϵ be the outage probability constraint of the typical link, i.e., $\mathbb{P}_{out}(d,T) = 1-\mathbb{P}_{suc}(d,T) \le \epsilon$, then the transmission capacity is given by

$$TC(d,\epsilon) = \max_{(\lambda,T):\mathbb{P}_{out}\leq\epsilon} \lambda \log(1+T)(1-\epsilon), \tag{36}$$

where λ is the transmission link density, which is $p\lambda_p$ for a half duplex network and $2p\lambda_p$ for a full duplex network.

Eq. (36) is a two-dimensional optimization problem, which is rather complicated. Instead of getting an optimal result for both λ and T, we are more interested in specific scenarios where either λ or T is fixed. When transmission link density is fixed, we have the following transmission capacity:

$$TC(d,\lambda_p,\epsilon) = \begin{cases} \max_{T:\mathbb{P}_{out}^{half}\leq\epsilon} p\lambda_p(1-\epsilon)\log(1+T), & \text{Half Duplex} \\ \max_{T:\mathbb{P}_{out}^{full}\leq\epsilon} 2p\lambda_p(1-\epsilon)\log(1+T), & \text{Full Duplex.} \end{cases}$$

When the transmission rate is fixed, we have the following transmission capacity:

$$TC(d,T,\epsilon) = \begin{cases} \max_{\lambda_p:\mathbb{P}_{out}^{half}\leq\epsilon} p\lambda_p(1-\epsilon)\log(1+T), & \text{Half Duplex} \\ \max_{\lambda_p:\mathbb{P}_{out}^{full}\leq\epsilon} 2p\lambda_p(1-\epsilon)\log(1+T), & \text{Full Duplex.} \end{cases}$$

In this case, the transmission capacity can be derived in a closed-form.

$$TC(d,T,\epsilon) = \begin{cases} \frac{(1-\epsilon)\ln(1-\epsilon)\log(1+T)}{\alpha^H(d,T)}, & \text{Half Duplex} \\ \frac{2(1-\epsilon)\ln(1-\epsilon)\log(1+T)}{\alpha^F(d,T)}, & \text{Full Duplex.} \end{cases}$$

From Lemma 5, it can be concluded that

$$TC^{Half}(d,T,\epsilon) \leq TC^{Full}(d,T,\epsilon) \leq 2TC^{Half}(d,T,\epsilon).$$

6 Numerical Results

In this section, numerical results of transmission throughput and transmission capacity are presented for both half duplex and full duplex wireless networks. A few common parameters fixed throughout the numerical analysis are given as follows. For a normal distribution function, the variance $\sigma^2 = \frac{1}{16}$. The path-loss function is $g(\mathbf{x}) = \frac{1}{\|\mathbf{x}\|^\alpha}$ with $\alpha = 4$. Distance of the typical link is set to the mean value, i.e., $\sqrt{\pi}\sigma$. Outage probability constraint corresponding to the transmission capacity is set to $\epsilon = 0.02$.

6.1 Transmission Capacity under Optimal Transmission Rate and Fixed Network Density

Network topology is the same for both half duplex and full duplex communications, and network throughput is maximized by optimizing the transmission rate to obtain the transmission capacity. To show different transmission capacity versus network density, the network density varies from 0.0001 to 0.25.

The maximum transmission rates for half duplex communications and full duplex communications are shown in Fig. 3. As the network density increases, the transmission rate decreases in both half duplex and full duplex communications, because a higher network density causes more aggregate interference. Since there exist more transmissions in full duplex communication under the same network density, the aggregate interference in full duplex communications is more severe than that in half duplex communications. Thus, the maximum transmission rate in full duplex communications is lower than that in half duplex communications. As shown in Fig. 3, the gap of the maximum transmission rate between half duplex and full duplex communications becomes larger as the network density increases.

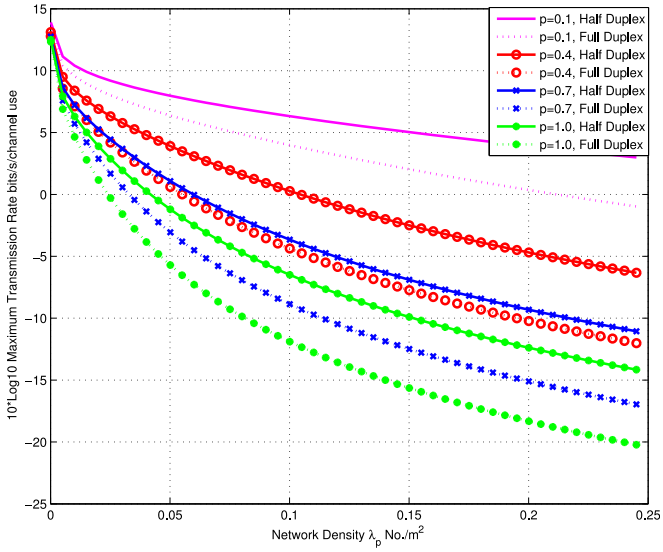

Fig. 3. Transmission rate of full duplex and half duplex communications under different network densities.

In Fig. 4, transmission capacities with respect to four access probabilities are shown. In all cases, the transmission capacity increases as the network density increases in the low network density region, but decreases in the high network density region. The reason is as follows. The aggregate interference increases as the network density increases. In the low network density region, the aggregate interference is light, so the reduced maximum transmission rate does not weight more than the increased network density, which leads to increasing transmission capacity. However, in the high network density region, severe aggregate interference reduces the transmission rate heavily, which weighs more than the network density and results in drop of transmission capacity.

Three points are marked in each sub-figure of Fig. 4: two max-capacity points where the maximum transmission capacity with respect to the network density is obtained and one equal-capacity point where the transmission capacities of two wireless networks are equal. For example, when $p = 0.1$, the max-capacity points are A1 and A2 for a full duplex and a half duplex wireless network, respectively, while the equal-capacity point is A, as depicted in Fig. 4a. In all scenarios with access probabilities $p = 0.1$, 0.4, 0.7 and 1.0, the max-capacity point of a full duplex network is always located at the left side of the max-capacity point of a half duplex network, which means the capacity reaches a maximum value at a lower network density in a full duplex wireless network. The reason is that a full duplex link includes two active transmitters, so the aggregate interference is more severe in a full duplex network under the same network density. Moreover, as the access probability p increases, the network density corresponding to the maximum capacity, i.e., the x-coordinate of the max-capacity

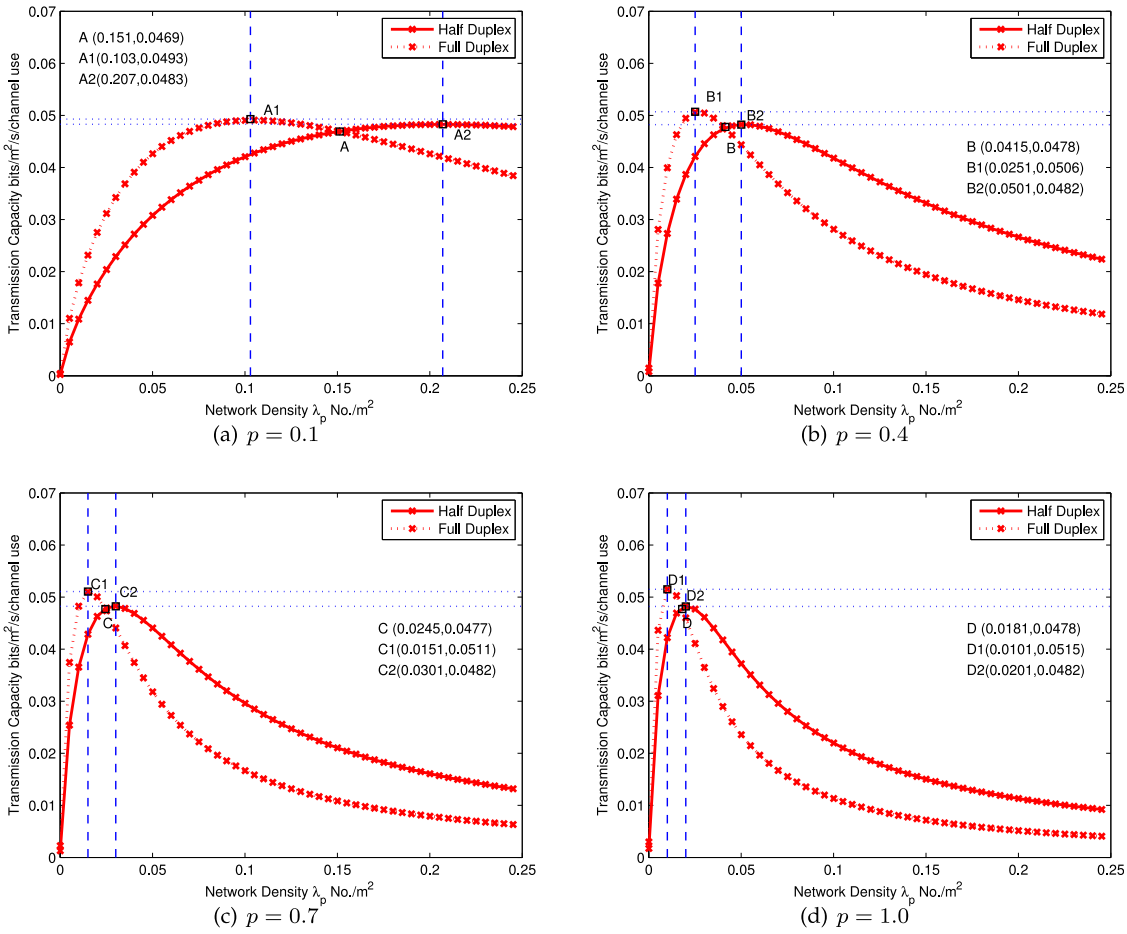

Fig. 4. Transmission capacity by maximizing transmission rate with a fixed network density.

point, decreases. For full duplex communications, such max-capacity network densities are 0.103, 0.0251, 0.0151 and 0.0101, respectively. For half duplex communications, the max-capacity network densities are 0.201, 0.0501, 0.0301 and 0.0201, respectively. The reason for these results is simple: a higher transmission probability p means more active transmitters under the same network density, so the transmission capacity saturates at a lower network density.

In Fig. 4 we notice that the network density at the maximum transmission capacity in each sub-figure is inversely proportional to the probability p. For example, $A1/D1 = 1.0/0.1 = 10$ and $A2/D2 = 10$. The reason for such an interesting result is explained as follows. Let $\lambda' = p\lambda_p$, the maximum transmission capacity can be determined with the following optimization problem:

$$TC_{\max}^{Full} = \max_{\lambda'} \max_{T} [\lambda' \log(1+T)(1-\epsilon)]$$
$$s.t. \exp\left\{-\lambda' \int_{\mathbb{R}^2} \left[1-\beta^2(\mathbf{x};d,T)\right] d\mathbf{x}\right\} \geq (1-\epsilon),$$

where the variables are defined in Section 5.4. When the maximum transmission capacity is achieved, λ' is located at the optimal point $\lambda^{*'}$, which is a constant. In other words, $p\lambda_p$ is the same when the transmission capacity reaches the maximum, which is consistent with the results in Fig. 4.

As shown in Fig. 4, with a larger access probability, the equal-capacity point corresponds to a lower network density. This means that, when the access probability increases, a full duplex network loses its advantage over a half duplex network at a lower network density, due to more severe interference experienced by full duplex links.

Based on Fig. 4, the transmission capacity ratio between full duplex and half duplex networks is presented in Fig. 5. It decreases from 2 to a number less than 0.6 as network density increases. Given a fixed network density, full duplex communications outperforms half duplex only in the low network density region, but lose the capacity gain in the high network density region. Moreover, the equal-capacity network density λ_p^t, i.e., the x-coordinate of the equal-capacity points (A, B, C, and D in Fig. 5), clearly decreases as transmission probability p increases.

6.2 Transmission Capacity under Optimal Network Density and Fixed Transmission Rate

The transmission rate is fixed and the transmission throughput is maximized with respect to the network density to obtain the transmission capacity.

To obtain the transmission capacity, the maximum network density under a certain transmission rate is shown in Fig. 6. Under the same transmission probability p, a transmission rate that corresponds to the transmission capacity is higher at a lower network density but lower at a high network density. This result is due to more severe aggregate interference in a network with a higher network density, which is consistent with the results in Section 6.1.

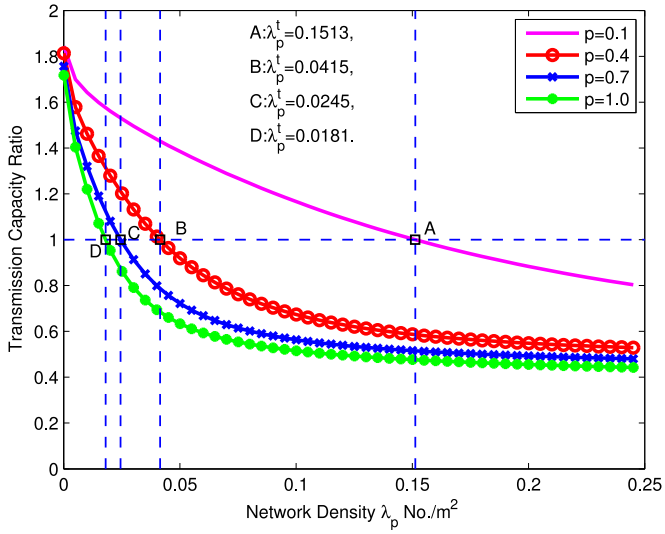

Fig. 5. Transmission capacity ratio between full duplex and half duplex under different network densities.

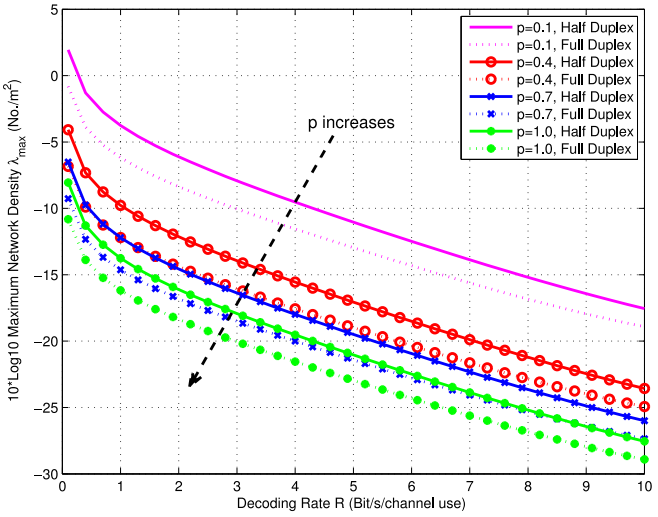

Fig. 6. Network density of full duplex and half duplex under different transmission rate.

In Fig. 6 we also notice that the plots at different values of p are just a shifted version of one another. The reason is explained below. Considering a fixed transmission rate, when the transmission capacity is achieved, the optimal value of $p\lambda_p$ is a fixed value.

Corresponding to Fig. 6, the transmission capacity versus the transmission rate is shown in Fig. 7a. It should be noted that the transmission capacity in this case does not change with a different transmission probability p. The reason is that the maximum density of active transmitters that the network can support remains unchanged under different transmission probabilities p. For a different transmission probability, the network density is optimized to reach the same maximum number of active transmitters to obtain the transmission capacity under a fixed transmission rate. Thus, transmission probability does not affect transmission capacity.

As shown in in Fig. 7a, for both half duplex and full duplex communications, if the network is in the low transmission rate region, then the optimized network density is very high. The reason is that nodes can tolerate high interference under a low transmission rate. However, due to low transmission rate, the overall transmission capacity is low. When the network is in the high transmission rate region, then the network density needs to be low to reduce interference, which also makes the overall transmission capacity low. As a result, when the transmission rate increases from the low region to the high region, the transmission capacity increases at first and then decreases. In other words, there exists an optimal point of the transmission rate (and its corresponding network density) to achieve the maximum transmission capacity, as depicted by points A and B for full duplex and half duplex wireless networks, respectively, in Fig. 7a.

Based on results in Fig. 7a, the transmission capacity ratio is depicted in Fig. 7b. We find that the transmission capacity of full duplex communications is always larger than that of half duplex communications under the same transmission rate requirement. Moreover, transmission capacity ratio varies from 1.00 to 1.46, indicating that the network capacity gain from full duplex communications is limited in a large scale wireless network.

7 Discussion

The analytical work conducted in this paper is an information-theoretic approach in which no collision awareness is considered. However, our analytical results are actually consistent with the results in existing work (e.g., [12], [18]) and are not counterintuitive.

The work in [12] is based on asymptotic analysis and takes the protocol model to consider active transmissions. The results (i.e., [12, Fig. 10]) indicate that the upper-bound of the capacity gain (i.e., the ratio between full duplex and half duplex wireless networks) is very limited unless the interference range is more than twice of the communication range. However, when the interference range is large, it means the density of active transmitters is low, i.e., the node density λ_p in our model is small. In this case, our analytical results also show that the capacity gain is much higher, which is consistent with the result in [12].

The analysis in [18] takes a stochastic geometry approach where one node of a full duplex link follows a Poisson point process and the other node is located within a fixed distance.[2] The analytical results (i.e., [18, Fig. 11]) show that, with an optimal sensing range of 200 meters, the capacity gain decreases quickly as the communication distance increases. For example, if the communication distance increases to be more than 100 meters, the gain is lower than 1.3. This result matches our analytical results. In fact, given a certain sensing range, a large communication distance in [18, Fig. 11] corresponds to the scenario of a dense network density in our analytical model, where the capacity gain decreases to a low level.

How to take into account collision awareness in an information-theoretical framework is an interesting but challenging research topic, which is subject to future research.

To show that our analytical results are not counterintuitive, we take the following simple example to illustrate a simple cause for limited capacity gain in a large scale wireless network. A multihop wireless network with a chain

2. The case of random distance is evaluated via simulations in [18].

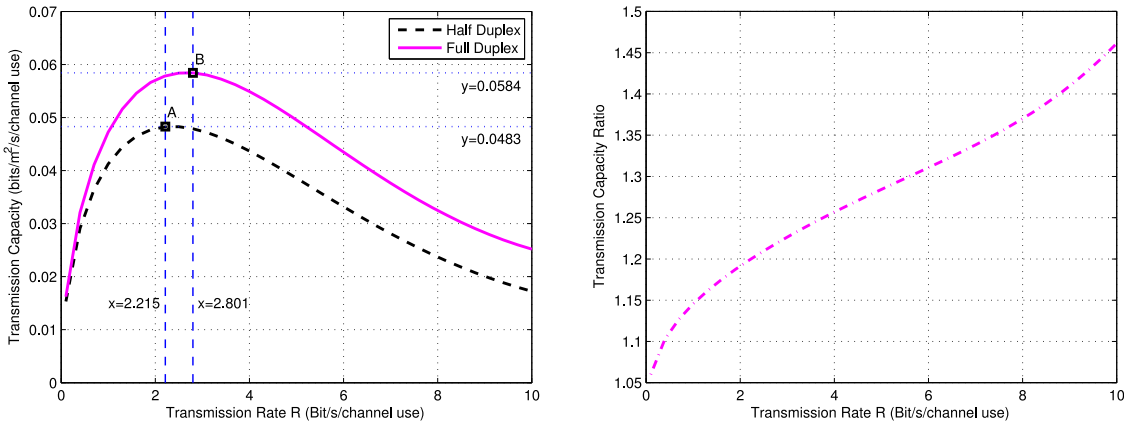

(a) Transmission capacity. (b) Transmission capacity ratio.

Fig. 7. Transmission capacity by maximizing the network density under a fixed transmission rate.

topology is considered in Fig. 8. We assume the interference range is between one hop and two hops of the communication range. When symmetrical full duplex communications are considered as shown in Fig. 8a, only two data links (i.e., symmetrical full duplex links between C and D) can be supported. All other links have to be held off to avoid interference to C and D. In the case of asymmetrical full duplex communications as shown in Fig. 8b, three links (i.e., C→D→E and A→B) can be supported, and other links have to be held off. In contrast, in the case of half duplex communications shown in Fig. 8b, three links (i.e., B→A, C→D, and F→E) can also be supported. Thus, in this chain topology setup, full duplex communications does not really bring any capacity gain.

Recently a full duplex radio called FlexRadio is developed in [24]. As compared to MIMO or full duplex communications, it can achieve additional capacity gain through interference nullifying and interference alignment. The capacity gain is demonstrated under a specific network network (i.e., [24, Fig. 1]), where three data streams can be supported simultaneously, while full duplex or MIMO can only support two data streams. Such additional capacity again shows the advantage of integrating full duplex with multiuser MIMO plus interference alignment. However, one critical point should be noted: FlexRadio is not really scalable to a large scale wireless network, as explained below.

We extend the network topology in [24] by adding one node, as shown in Fig. 9a. In this new network setup, only three data streams (i.e., A→B, A→C, and B→D) can be supported. The communication link from D to E (i.e., D→E) cannot be supported, due to the interference from D to both B and C. Link E→D cannot be supported either, since D receives data from B. Under the same network setup, if half duplex is considered, it can also support three data streams (i.e., A→B, A→C, and E→D), because A→B and A→C are supported through multiuser MIMO and are not interfered by E→D. Thus, full duplex does not bring any capacity gain in this particular network setup. Considering a large scale wireless network, many such scenarios exist. Thus, the capacity gain from full duplex is limited, even if FlexRadio is adopted.

The examples of the chain-topology network and FlexRadio show that full duplex itself does not ensure scalable capacity in a large wireless network, which is exactly what our analytical results reveal. Even if Flexradio is adopted, the scalability of full duplex communications is not necessarily maintained. However, Flexradio does illustrate the potential benefits of integrating full duplex communications with interference alignment in certain network setup.

8 Conclusion

In this paper, the aggregate interference and the transmission capacity of a full duplex wireless network were studied via stochastic geometry. Analytical results illustrated two interesting properties of the aggregate interference: 1) The asymptotic order of tail probability of the aggregate interference in a full duplex wireless network is the same as that in a half duplex network; 2) The aggregate interference in a full duplex network is more dispersed than that in a half duplex wireless network. Results also showed that, the transmission

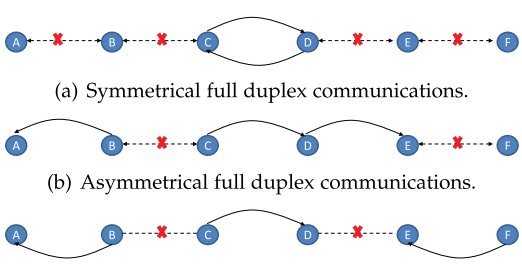

(a) Symmetrical full duplex communications.

(b) Asymmetrical full duplex communications.

(c) Half duplex communications.

Fig. 8. Comparisons between full duplex and half duplex data streams in a chain-topology wireless network.

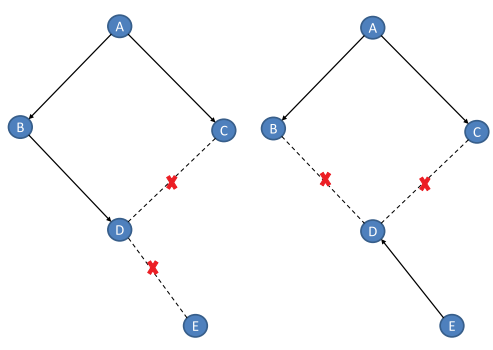

(a) Full duplex (b) Half duplex

Fig. 9. Comparisons of data streams between full duplex and half duplex radios.

capacity of a full duplex wireless network outperforms that of a half duplex wireless network in a low transmission rate region, but the transmission capacity gain is limited. Moreover, in a high transmission rate region, the performance of a full duplex wireless network is even lower than that of a half duplex wireless network. The major reason for this issue is that the aggregate interference is more severe in full duplex communications. Low capacity gain from full duplex communications in a large scale wireless network indicates the importance of developing mutual-interference cancellation techniques for a full duplex wireless network. Capacity analysis considering both self-interference cancellation, mutual-interference cancellation, and interference alignment is an interesting topic for future research.

Acknowledgments

The authors would like to thank Professor Radha Krishna Ganti from IIT Madras, Chennai, India, for his discussions on the properties of the Thomas cluster point process. They also appreciate the constructive comments and suggestions from the editor and the anonymous reviewers. The research work is supported by ZTE Cooperation and National Natural Science Foundation of China (NSFC) No. 61172066. They would like to thank these sponsors for their generous support.

References

[1] E. Everett, M. Duarte, C. Dick, and A. Sabharwal, "Empowering full-duplex wireless communication by exploiting directional diversity," in *Proc. Conf. Rec. 45th Asilomar Conf. Signals, Syst. Comput.*, 2011, pp. 2002–2006.

[2] J. I. Choi, M. Jain, K. Srinivasan, P. Levis, and S. Katti, "Achieving single channel, full duplex wireless communication," in *Proc. 16th Annu. Int. Conf. Mobile Comput. Netw.*, 2010, pp. 1–12.

[3] B. Radunovic, D. Gunawardena, P. Key, A. Proutiere, N. Singh, V. Balan, and G. Dejean, "Rethinking indoor wireless mesh design: Low power, low frequency, Full-duplex," in *Proc. 5th IEEE Workshop Wireless Mesh Netw.*, 2010, pp. 1–6.

[4] M. Jain, J. I. Choi, T. Kim, D. Bharadia, S. Seth, K. Srinivasan, P. Levis, S. Katti, and P. Sinha, "Practical, Real-time, full duplex wireless," in *Proc. 17th Annu. Int. Conf. Mobile Comput. Netw.*, 2011, pp. 301–312.

[5] E. Aryafar, M. A. Khojastepour, K. Sundaresan, S. Rangarajan, and M. Chiang, "MIDU: Enabling MIMO full duplex," in *Proc. 18th Annu. Int. Conf. Mobile Comput. Netw.*, 2012, pp. 257–268.

[6] D. Bharadia, E. McMilin, and S. Katti, "Full duplex radios," in *Proc. ACM SIGCOMM Conf.*, 2013, pp. 375–386.

[7] J. Bai and A. Sabharwal, "Distributed full-duplex via wireless side-channels: Bounds and protocols," *IEEE Trans. Wireless Commun.*, vol. 12, no. 8, pp. 4162–4173, Aug. 2013.

[8] S. Barghi, A. Khojastepour, K. Sundaresan, and S. Rangarajan, "Characterizing the throughput gain of single cell mimo wireless systems with full duplex radios," in *Proc. 10th Int. Symp. Model. Optimization Mobile, Ad Hoc Wireless Netw.*, 2012, pp. 68–74.

[9] B. Radunovic, D. Gunawardena, A. Proutiere, N. Singh, V. Balan, and P. Key, "Efficiency and fairness in distributed wireless networks through Self-interference cancellation and scheduling," Microsoft Res., Redmond, WA, USA, Tech. Rep. MSR-TR-2009-27, 2009.

[10] S. Kim and W. E. Stark, "On the performance of full duplex wireless networks," in *Proc. 47th Annu. Conf. Inf. Sci. Syst.*, 2013, pp. 1–6.

[11] H. Ju, S. Lim, D. Kim, H. V. Poor, and D. Hong, "Full duplexity in beamforming-based multi-hop relay networks," *IEEE J. Sel. Areas Commun.*, vol. 30, no. 8, pp. 1554–1565, Sep. 2012.

[12] X. Xie and X. Zhang, "Does Full-duplex double the capacity of wireless networks?" in *Proc. IEEE INFOCOM*, 2014, pp. 253–261.

[13] D. Stoyan, W. S. Kendall, J. Mecke, and L. Ruschendorf, *Stochastic Geometry and Its Applications*, vol. 2. Chichester, U.K.: Wiley, 1995.

[14] S. P. Weber, X. Yang, J. G. Andrews, and G. De Veciana, "Transmission capacity of wireless ad hoc networks with outage constraints," *IEEE Trans. Inf. Theory*, vol. 51, no. 12, pp. 4091–4102, Dec. 2005.

[15] M. Z. Win, P. C. Pinto, and L. A. Shepp, "A mathematical theory of network interference and its applications," *Proc. IEEE*, vol. 97, no. 2, pp. 205–230, Feb. 2009.

[16] R. K. Ganti and M. Haenggi, "Interference and outage in clustered wireless ad hoc networks," *IEEE Trans. Inf. Theory*, vol. 55, no. 9, pp. 4067–4086, Sep. 2009.

[17] Y. Yang, B. Chen, K. Srinivasan, and N. B. Shroff, "Characterizing the achievable throughput in wireless networks with two active RF chains," in *Proc. IEEE INFOCOM*, 2014, pp. 262–270.

[18] S. Wang, V. Venkateswaran, and X. Zhang, "Exploring full-duplex gains in multi-cell wireless networks: A spatial stochastic framework," in *Proc. IEEE INFOCOM*, 2015, pp. 855–863.

[19] F. Baccelli, B. Blaszczyszyn, and P. Muhlethaler, "An Aloha protocol for multihop mobile wireless networks," *IEEE Trans. Inf. Theory*, vol. 52, no. 2, pp. 421–436, Feb. 2006.

[20] M. Haenggi, J. G. Andrews, F. Baccelli, O. Dousse, and M. Franceschetti, "Stochastic geometry and random graphs for the analysis and design of wireless networks," *IEEE J. Sel. Areas Commun.*, vol. 27, no. 7, pp. 1029–1046, Sep. 2009.

[21] R. Ganti and M. Haenggi, "Interference in ad hoc networks with general Motion-invariant node distributions," in *Proc. IEEE Int. Symp. Inf. Theory*, Jul. 2008, pp. 1–5.

[22] R. Ganti and M. Haenggi, "Spatial and temporal correlation of the interference in ALOHA ad hoc networks," *IEEE Commun. Lett.*, vol. 13, pp. 631–633, Sep. 2009.

[23] M. Haenggi, *Stochastic Geometry for Wireless Networks*. Cambridge, U.K.: Cambridge Univ. Press, 2012.

[24] B. Chen, V. Yenamandra, and K. Srinivasan,, "FlexRadio: Fully flexible radios," in *Proc. 12th USENIX Symp. Netw. Syst. Des. Implementation*, 2015, pp. 205–218.

Xudong Wang received the PhD degree in electrical and computer engineering from Georgia Institute of Technology in August 2003. He is currently with the UM-SJTU Joint Institute, Shanghai Jiao Tong University. He is a distinguished professor (Shanghai Oriental Scholar) and is the director in the Wireless and NetworkinG (WANG) Lab. He is also an affiliate faculty member with the Electrical Engineering Department, University of Washington. He has been working as a senior research engineer, senior network architect, and R&D manager in several companies. He has been actively involved in R&D, technology transfer, and commercialization of various wireless networking technologies. His research interests include wireless communication networks, smart grid, and cyber physical systems. He holds several patents on wireless networking technologies and most of his inventions have been successfully transferred to products. He is an editor of the *IEEE Transactions on Mobile Computing*, *IEEE Transactions on Vehicular Technology*, and Elsevier *Ad Hoc Networks*. He was the demo co-chair of the ACM International Symposium on Mobile Ad Hoc Networking and Computing (ACM MOBIHOC 2006), a technical program co-chair of Wireless Internet Conference (WICON) 2007, and a general co-chair of WICON 2008. He has been a technical committee member of many international conferences. He is a senior member of the IEEE.

Huaiyu Huang received the MS degree in electrical and computer engineering from Shanghai Jiao Tong University (SJTU), Shanghai, China, in 2014. He is currently a research engineer with the Signal Processing Department, Nanjing Research Institute of Electronics Technology, Nanjing, China. His research interests include wireless communications, wireless networks, and radar signal processing.

Taewon Hwang received the BS degree in electrical and electronic engineering from Yonsei University, Seoul, Korea, in 1993. He received the MS degree in electrical and computer engineering from Georgia Institute of Technology, Atlanta, GA, in 1995, and the PhD degree from the Department of Electrical and Computer Engineering, Georgia Institute of Technology in 2005. From 1995 to 2000, he was a member of Technical Staff at the Electronics and Telecommunications Research Institute (ETRI), Daejeon, Korea. Since 2006, he has been with the School of Electrical and Electronic Engineering at Yonsei University, Seoul, Korea, where he is currently an associate professor. His research interests include energy-efficient communications, cognitive radio, and MIMO communications. He has been a technical program committee member of many international conferences. Also, he served as an editor of the *IEEE Journal on Selected Areas on Communications: Cognitive Radio Series*.